Journal of Applied Mechanics Vol.7,pp.997-1004 (August 2004) JSCE

Linear stability analysis of channel inception on slopes with arbitrary shapes: purely erosional case

任意形状を有する斜面上における水路形成の線形安定論: 侵食が卓越する場合

Adichai PORNPROMMIN*, Norihiro IZUMI** and Tetsuro TSUJIMOTO***
アディチャイポンプロミン, 泉 典洋, 辻本哲郎

*M.Eng., Doctoral Student, Dept. Geotech. & Env. Eng. Nagoya Univ.
(Chikusa-ku, Nagoya 464-8603)
**Ph.D., Associate Professor, Dept. Civil Eng. Tohoku Univ.
***D.Eng., Professor, Dept. Geotech. & Env. Eng. Nagoya Univ.

The existing linear stability analysis of incipient channelization was limited to the case of self-preserving slope profiles. In this study, the theory is extended to include the channelization on slopes with arbitrary shapes under the assumption that the growth of perturbation is sufficiently faster than the evolution of base state slope profiles; thus, a time derivative term in base state equations is neglected in the linear level (frozen time approach). As the result of a momentary stability analysis, the dominant wavelength is found to decrease with increasing curvature of slopes. In addition, the analysis shows the possibility of channelization even in the case of arbitrary slope profiles.

Key Words : *channelization, arbitrary shapes, frozen time approach, linear stability analysis, momentary stability, pure erosion*

1. Introduction

Since the first theoretical analysis of channel inception on hillslopes by Smith and Bretherton[1], a large number of studies have been proposed. In some of the recent studies[2),3),4)], Izumi and Parker's[3)] analysis may deserve special mention. They performed a linear stability analysis to provide a physical explanation on the formation of gullies commonly observed to be uniformly spaced at the edge of plateaus. According to their analysis, the spacing is on the order of one thousand times the depth of sheet flow on plateaus. Their result provides a reasonable explanation for the gully spacing observed in the field.

Their linear stability analysis was limited to the case of self-preserving slope profiles, which are considered to be fully-developed unchannelized slope profiles. If no channelization takes place, an arbitrary base profile evolves into a self-preserving profile which preserves its shape and migrates upstream at a constant speed due to erosion. However, there is no reason to deny that channelization takes place even before the slope profile becomes the self-preserving profile. In that case, the slope profile does not satisfy the self-preserving conditions, so that the existing analysis is not applicable. In order to investigate the channelization on slopes with arbitrary shapes at a given instant, we have to deal with linear stability analysis involving the temporal evolution of the base state.

In this study, the theory is extended to include the channelization on slopes with arbitrary shapes with the use of the frozen time approach and the momentary stability concept. The frozen time approach assumes that the growth of perturbations is sufficiently faster than the evolution of basic arbitrary shapes, so that time-dependent terms of the base state can be neglected in linear stability analysis. With this assumption, the instability of instantaneous arbitrary shapes is analyzed in a fashion similar to the analysis for the self-preserving problem. However, the growth or decay of disturbances is meaningful only in comparison with the growth or decay of the evolving base state. We adopt the concept of "momentary stability" by Shen[5)] and others[6),7)]. Shen introduced a more general definition of instability, in which, if a disturbance grows faster than the evolution of the base state, the disturbance is amplified in time. This is referred to as "momentarily unstable" in his paper.

2. Formulation

2.1 Governing equations

Let us consider sheet flow on a slope with an arbitrary shape as shown in Fig. 1. Since the scale of the lateral direction is sufficiently large, we employ the

¶ Dedicated to the memory of Prof. Michihiro KITAHARA

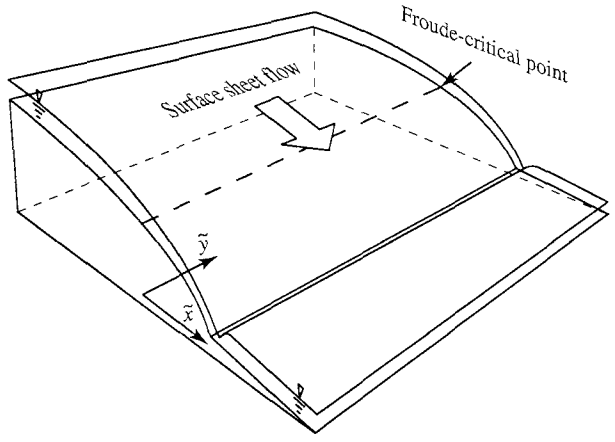

Fig. 1 A slope with an arbitrary shape and flow on the slope.

depth-averaged St. Venant equations of shallow water flow in the analysis. In addition, we adopt the quasi-steady assumption in which the time variation of the bed is far slower than that of flow, so that the time derivative terms can be neglected in the flow equations. Then the flow can be described by

$$\tilde{u}\frac{\partial \tilde{u}}{\partial \tilde{x}} + \tilde{v}\frac{\partial \tilde{u}}{\partial \tilde{y}} = -g\frac{\partial \tilde{h}}{\partial \tilde{x}} - g\frac{\partial \tilde{\eta}}{\partial \tilde{x}} - \frac{\tilde{\tau}_x}{\rho \tilde{h}} \tag{1}$$

$$\tilde{u}\frac{\partial \tilde{v}}{\partial \tilde{x}} + \tilde{v}\frac{\partial \tilde{v}}{\partial \tilde{y}} = -g\frac{\partial \tilde{h}}{\partial \tilde{y}} - g\frac{\partial \tilde{\eta}}{\partial \tilde{y}} - \frac{\tilde{\tau}_y}{\rho \tilde{h}} \tag{2}$$

$$\frac{\partial \tilde{u}\tilde{h}}{\partial \tilde{x}} + \frac{\partial \tilde{v}\tilde{h}}{\partial \tilde{y}} = 0 \tag{3}$$

where $\tilde{}$ means the dimensional variables, $\tilde{x}$ and $\tilde{y}$ are the streamwise and lateral coordinates respectively, $\tilde{u}$ and $\tilde{v}$ are the $\tilde{x}$ and $\tilde{y}$ components of velocity respectively, $\tilde{h}$ and $\tilde{\eta}$ are the flow depth and the bed elevation respectively, $\tilde{\tau}_x$ and $\tilde{\tau}_y$ are the $\tilde{x}$ and $\tilde{y}$ components of bed shear stress respectively, ρ is the water density, and g is the gravity acceleration.

The bed shear stress vector $(\tilde{\tau}_x, \tilde{\tau}_y)$ is written as

$$(\tilde{\tau}_x, \tilde{\tau}_y) = \rho C_f \left(\tilde{u}^2 + \tilde{v}^2\right)^{1/2} (\tilde{u}, \tilde{v}) \tag{4}$$

where C_f is a friction coefficient and assumed to be a constant for simplicity.

In this study, a purely erosional formulation is employed; thus, the effects of deposition is ignored. This formulation is applicable when the erosion rate is sufficiently small, and storm-driven flows have a capacity to transport sediment on slopes far downstream. With this in mind, the Exner equation of the conservation of bed sediment takes the form

$$\frac{\partial \tilde{\eta}}{\partial \tilde{t}} = -\tilde{E}(\tilde{\tau}) \tag{5}$$

where $\tilde{E}$ denotes the erosion rate of the bed due to the flow of water. It is normally approximated by the form

$$\tilde{E}(\tilde{\tau}) = \begin{cases} \alpha((\tilde{\tau}/\tilde{\tau}_{th}) - 1)^{\gamma} & \text{if} \quad \tilde{\tau} \geq \tilde{\tau}_{th} \\ 0 & \text{if} \quad \tilde{\tau} < \tilde{\tau}_{th} \end{cases} \tag{6}$$

$$\tilde{\tau} = (\tilde{\tau}_x^2 + \tilde{\tau}_y^2)^{1/2} \tag{7}$$

where $\tilde{\tau}_{th}$ denotes the threshold value of $\tilde{\tau}$ for the onset of bed erosion, γ denotes a dimensionless exponent and α is a parameter with the dimension of velocity.

The domain of solution is $(-\infty, \tilde{x}_c)$ where $\tilde{x}_c$ denotes the point at which Froude critical condition is achieved. Appropriate upstream and downstream conditions can be set as follows. Far upstream from the Froude critical point, the slope is assumed to be a constant S_n, so that the flow should attain steady, uniform normal conditions. Thus, we have

$$(\tilde{u}, \tilde{v}) \to (\tilde{u}_n, 0), \quad -\frac{\partial \tilde{\eta}}{\partial \tilde{x}} \to S_n \quad \text{as} \quad \tilde{x} \to -\infty \tag{8a,b}$$

where $\tilde{u}_n$ is the velocity in the normal condition, derived from

$$C_f \tilde{u}_n^2 = g\tilde{h}_n S_n, \quad \tilde{u}_n \tilde{h}_n = \tilde{q} \tag{9a,b}$$

where $\tilde{q}$ is a constant water discharge per unit width.

When the bed shape becomes steeper in the downstream direction, the Froude critical condition is achieved at some point $\tilde{x}_c$, where the bed elevation $\tilde{\eta}$ is taken to vanish for convenience. It follows that

$$Fr = 1, \quad \tilde{\eta} = 0 \quad \text{at} \quad \tilde{x} = \tilde{x}_c \tag{10a,b}$$

where the Froude number Fr is denoted as

$$Fr = \left(\frac{\tilde{u}^2 + \tilde{v}^2}{g\tilde{h}}\right)^{1/2} \tag{11}$$

and $\tilde{x}_c$ is set to be zero without losing generality.

2.2 Non-dimensionalization

The following non-dimensionalizations are introduced. The variables without tildes are the dimensionless version of the corresponding variables with tildes.

$$(\tilde{u}, \tilde{v}) = \tilde{U}_c(u, v), \quad (\tilde{x}, \tilde{y}) = \frac{\tilde{D}_c}{C_f}(x, y) \tag{12a,b}$$

$$(\tilde{h}, \tilde{\eta}) = \tilde{D}_c(h, \eta), \quad \tilde{k} = \left(\frac{\tilde{D}_c}{C_f}\right)^{-1} k \tag{12c,d}$$

$$\tilde{t} = \tilde{D}_c \left[\alpha \left(\frac{\tilde{\tau}_c}{\tilde{\tau}_{th}}\right)^{\gamma}\right]^{-1} t, \quad \tilde{\tau}_c = \rho C_f \tilde{U}_c^2 \tag{12e,f}$$

where the subscript c denotes the Froude critical condition.

Introducing Eqs. (12a–f) into Eqs. (1)–(3) and (5) and reducing, the following dimensionless relations are obtained:

$$u\frac{\partial u}{\partial x} + v\frac{\partial u}{\partial y} = -\frac{\partial h}{\partial x} - \frac{\partial \eta}{\partial x} - \frac{\left(u^2 + v^2\right)^{1/2} u}{h} \tag{13}$$

$$u\frac{\partial v}{\partial x}+v\frac{\partial v}{\partial y}=-\frac{\partial h}{\partial y}-\frac{\partial \eta}{\partial y}-\frac{\left(u^2+v^2\right)^{1/2}v}{h} \tag{14}$$

$$\frac{\partial uh}{\partial x}+\frac{\partial vh}{\partial y}=0 \tag{15}$$

$$\frac{\partial \eta}{\partial t}=-E(u^2+v^2) \tag{16}$$

The function E denotes the dimensionless rate of bed erosion, given by

$$E(u^2+v^2)=\begin{cases}(u^2+v^2-\psi)^{\gamma} & \text{if} \quad u^2+v^2\geq\psi\\ 0 & \text{if} \quad u^2+v^2<\psi\end{cases} \tag{17}$$

where ψ denotes the ratio of the critical shear stress for bed erosion to the shear stress at Froude critical condition:

$$\psi=\frac{\tilde{\tau}_{th}}{\tilde{\tau}_c} \tag{18}$$

The corresponding non-dimensionalization of Eqs. (8a, b) and (10a, b) yields the upstream and the downstream boundary conditions

$$(u,v)\to(u_n,0),\quad -\frac{\partial \eta}{\partial x}\to\sigma \quad \text{as} \quad x\to-\infty \tag{19a, b}$$

and

$$u^2+v^2=h,\quad \eta=0 \quad \text{at} \quad x=0 \tag{20a, b}$$

where σ denotes the normalized upstream slope ($=S_n/C_f$).

2.3 Coordinate transformation

We employ a linear coordinate transformation described by

$$t^*=t,\quad x^*=x+ct,\quad \eta^*=\eta-bt \tag{21a–c}$$

where $*$ denotes the moving coordinate corresponding to the migration speeds c and b in the horizontal and vertical directions, respectively.

Appropriate values of c and b are selected under two conditions. The first condition is to preserve the domain of the solution $(-\infty,\tilde{x}_c)$ in the temporal variation. Second condition is that the bed evolution far upstream should vanish and the normal flow condition should be achieved. The computation of c and b will be discussed in the next section.

With the use of the above coordinate transformation, the governing equations are rewritten in the forms

$$u\frac{\partial u}{\partial x}+v\frac{\partial u}{\partial y}=-\frac{\partial h}{\partial x}-\frac{\partial \eta}{\partial x}-\frac{\left(u^2+v^2\right)^{1/2}u}{h} \tag{22}$$

$$u\frac{\partial v}{\partial x}+v\frac{\partial v}{\partial y}=-\frac{\partial h}{\partial y}-\frac{\partial \eta}{\partial y}-\frac{\left(u^2+v^2\right)^{1/2}v}{h} \tag{23}$$

$$\frac{\partial uh}{\partial x}+\frac{\partial vh}{\partial y}=0 \tag{24}$$

$$\frac{\partial \eta}{\partial t}+c\frac{\partial \eta}{\partial x}+b=-E(u^2+v^2) \tag{25}$$

where $*$ is dropped for simplicity, herein and hereafter.

3. The one-dimensional base state

3.1 Formulation

In the one-dimensional base state, flow is considered to be uniform in the lateral direction; thus, the terms associated with the lateral direction are dropped. Then, the governing equations reduce to

$$u\frac{\partial u}{\partial x}+\frac{\partial h}{\partial x}+\frac{\partial \eta}{\partial x}+\frac{u^2}{h}=0 \tag{26}$$

$$uh=1 \tag{27}$$

$$\frac{\partial \eta}{\partial t}+c\frac{\partial \eta}{\partial x}+b+E(u^2)=0 \tag{28}$$

where

$$E(u^2)=\begin{cases}(u^2-\psi)^{\gamma} & \text{if} \quad u^2\geq\psi\\ 0 & \text{if} \quad u^2<\psi\end{cases} \tag{29}$$

3.2 Solution for arbitrary shapes

(1) Solution for flow

Since the base state profile is assumed arbitrarily, the solution of the flow can be achieved by substituting Eq. (27) into Eq. (26). Thus, we have

$$u'=-\frac{\eta'+u^3}{u-u^{-2}} \tag{30}$$

where $'$ denotes the partial derivative with respect to x.

At the Froude critical point, u takes a value of unity. It is found that the denominator of the above equation vanishes. In order for u' not to be infinity at the Froude critical point, the numerator has to vanish at once, such that

$$\eta'(0)=-1 \tag{31}$$

Applying L'hopitel's rule to Eq. (30), we have

$$u'(0)=\lim_{x\to0,u\to1}-\frac{\eta''+3u^2u'}{u'+2u^{-3}u'}=-\frac{\eta''(0)+3u'(0)}{3u'(0)} \tag{32}$$

The solution of the above equation is

$$u'(0)=\frac{1}{2}\left\{-1\pm\sqrt{1-\frac{4}{3}\eta''(0)}\right\} \tag{33}$$

This implies that once the slope profile η is given, $u'(0)$ can be derived from the above equation. We are assuming the upward convex slope profile as shown in Fig. 1; therefore, $\eta''(0)$ is negative. On such a slope, the velocity should be accelerated in the streamwise direction, so that $u'(0)$ should be positive. Because of the above restrictions, Eq. (33) is reduced to

$$u'(0)=\frac{1}{2}\left\{-1+\sqrt{1-\frac{4}{3}\eta''(0)}\right\} \tag{34}$$

with the condition

$$\eta''(0)<0 \tag{35}$$

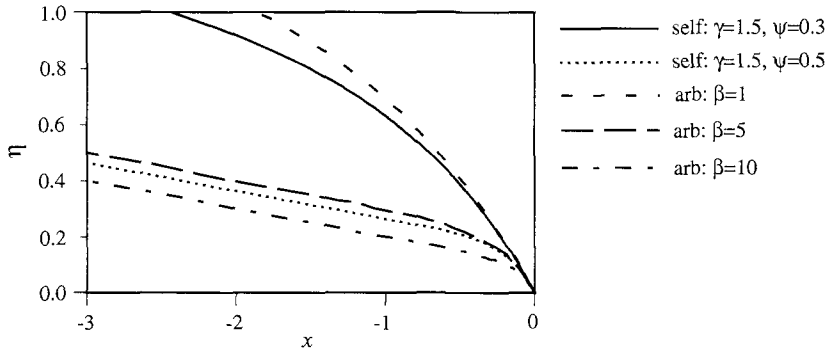

Fig. 2 Comparison of the bed profile between the self-preserving profiles and arbitrary shapes when $\sigma = 0.1$ ("self" denotes the self-preserving profile and "arb" denotes an arbitrary profile).

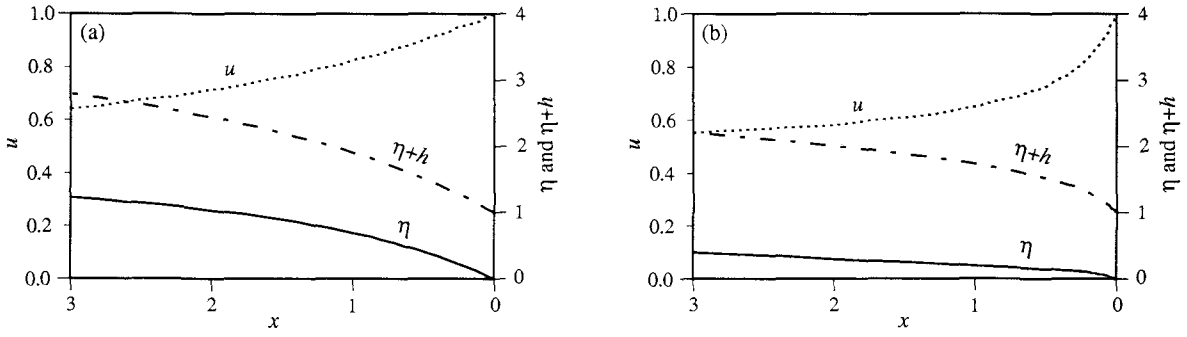

Fig. 3 The one-dimensional base state solutions u, h, $\eta + h$ for (a) $\sigma = 0.1$ and $\beta = 1$, and (b) $\sigma = 0.1$ and $\beta = 10$.

(2) Solution for the bed variation

As mentioned before, in order to preserve the domain of the solution $(-\infty, 0)$ in the temporal variation, Eq. (31) remains to be satisfied; therefore, the following condition has to be achieved at the Froude critical point:

$$\frac{\partial^2 \eta}{\partial x \partial t} = 0 \quad \text{at} \quad x = 0 \tag{36}$$

Taking the derivative of Eq. (28) with respect to x and with the use of the above condition, we obtain

$$c\frac{\partial^2 \eta}{\partial x^2} + E_u \frac{\partial u}{\partial x} = 0 \quad \text{at} \quad x = 0 \tag{37}$$

where E_u is the derivative of the dimensionless erosion rate with respect to u $(= \partial E/\partial u)$ described by

$$E_u(u^2) = \begin{cases} 2\gamma u(u^2 - \psi)^{\gamma - 1} & \text{if} \quad u^2 \geq \psi \\ 0 & \text{if} \quad u^2 < \psi \end{cases} \tag{38}$$

Evaluating the above equation at the Froude critical point, we have the following relation:

$$c\eta''(0) + E_u(1)u'(0) = 0 \tag{39}$$

Thus, the appropriate migration speed is derived from the above relation as

$$c = -\frac{E_u(1)u'(0)}{\eta''(0)}$$

$$= -\frac{\gamma(1-\psi)^{(\gamma-1)}}{\eta''(0)} \left\{ -1 + \sqrt{1 - \frac{4}{3}\eta''(0)} \right\} \tag{40}$$

The constant b can be obtained by considering flow far upstream where the time variation of the bed elevation vanishes and normal conditions are maintained; thus, we obtain

$$b = c\sigma - E_n \tag{41}$$

where E_n denotes the dimensionless erosion rate under the normal flow condition far upstream as

$$E_n = \begin{cases} (u_n^2 - \psi)^{\gamma} & \text{for} \quad u_n^2 \geq \psi \\ 0 & \text{for} \quad u_n^2 < \psi \end{cases} \tag{42}$$

3.3 Results and discussion of the base state

In this study, an arbitrary slope profile is assumed to be described by

$$\eta = -\sigma x - \frac{1}{\beta}\left[e^{\beta(1-\sigma)x} - 1 \right] \tag{43}$$

where β is a parameter representing the curvature of the profile. The slope is assumed to asymptotically approach the constant slope σ far upstream $(x \to -\infty)$. At the Froude critical point, the first and second derivatives of arbitrary shape are written, respectively, in the form

$$\eta'(0) = -1, \quad \eta''(0) = -\beta(1-\sigma)^2 \tag{44a, b}$$

It can be seen that, at the Froude critical point, the bed slope equals -1 corresponding to the condition of Eq. (31) and the curvature of the bed increases with the parameter β.

The comparison between arbitrary slope profiles and the self-preserving profiles is shown in Fig. 2. It is found that it requires longer distance for the slope to become a constant σ with decreasing β. If an appropriate value of β is selected, the arbitrary profile becomes close to the self-preserving profile.

The flow is solved numerically using Eq. (30) with the boundary condition (34). Some examples of the base state solution u, η and $\eta + h$ are shown in Fig. 3. We found that the flow is intensively accelerated near the Froude critical point with increasing β.

4. The two-dimensional perturbation problem

4.1 Linearization

The following perturbations are imposed on the slope profile:

$$\eta = \eta_0(x) + a\eta_1(x)\mathrm{e}^{\Omega t}\cos ky \tag{45}$$

Correspondingly, other variables are expanded as

$$u = u_0(x) + au_1(x)\mathrm{e}^{\Omega t}\cos ky \tag{46}$$

$$v = av_1(x)\mathrm{e}^{\Omega t}\sin ky \tag{47}$$

$$h = h_0(x) + ah_1(x)\mathrm{e}^{\Omega t}\cos ky \tag{48}$$

where a is the amplitude of the disturbance assumed to be small, Ω and k are the growth rate and the wavenumber of the disturbance, respectively.

Substituting the above equations into the governing equations (22)–(25), we have the following equations at $O(a)$:

$$\frac{\mathrm{d}u_1}{\mathrm{d}x} = \frac{(u_0^2 + u_0^{-1})u_0' + 2u_0^4 - c^{-1}E_u(u_0^2)u_0^2}{1 - u_0^3}u_1 - \frac{k}{1-u_0^3}v_1 - \frac{u_0u_0' + u_0^6}{1-u_0^3}h_1 - \frac{c^{-1}\Omega u_0^2}{1-u_0^3}\eta_1 \tag{49}$$

$$\frac{\mathrm{d}v_1}{\mathrm{d}x} = -u_0v_1 + \frac{k}{u_0}h_1 + \frac{k}{u_0}\eta_1 \tag{50}$$

$$\frac{\mathrm{d}h_1}{\mathrm{d}x} = -\frac{2u_0' + 2u_0^2 - c^{-1}E_u(u_0^2)}{1-u_0^3}u_1 + \frac{ku_0}{1-u_0^3}v_1 + \frac{u_0^4 + u_0^2u_0'}{1-u_0^3}h_1 + \frac{c^{-1}\Omega}{1-u_0^3}\eta_1 \tag{51}$$

$$\frac{\mathrm{d}\eta_1}{\mathrm{d}x} = -c^{-1}E_u(u_0^2)u_1 - c^{-1}\Omega\eta_1 \tag{52}$$

4.2 Boundary conditions

Far upstream from the Froude critical point, the flow asymptotically approaches to the normal flow condition, and the perturbations disappear, such that

$$u_1 = v_1 = h_1 = \eta_1 = 0 \quad \text{as} \quad x \to -\infty \tag{53a–d}$$

It appears that the above equations include four boundary conditions. However, as found in Eqs. (49)–(52), if three of the four boundary conditions hold, the rest is automatically satisfied. Thus, there are only three boundary conditions included in Eq. (53a–d).

At the Froude-critical point, the denominator on the right side of Eqs. (49) and (51) vanishes; thus, a singularity appears again. The regularity condition to prevent the equations from becoming infinity is that the numerator vanishes at once. Evaluating Eq. (49) with multiplied by $1 - u_0^3$ at the Froude-critical point, the following equation is required in order for $\mathrm{d}u_1/\mathrm{d}x$ to be finite:

$$\left(2u_0'(0) + 2 - c^{-1}E_u(1)\right)u_1 - kv_1 - \left(u_0'(0) + 1\right)h_1 - \Omega c^{-1}\eta_1 = 0 \quad \text{at} \quad x = 0 \tag{54}$$

Eqs. (49)–(52) are four first-order ordinary differential equations with respect to four unknowns u_1, v_1, h_1, η_1, and form an Sturm-Liouville type eigenvalue problem with an eigenvalue of Ω and the four boundary conditions (53a–d) and (54). In order to apply the relaxation method, we solve (49)–(52) as the nonlinear two-point boundary value problem by setting the bed elevation at the origin to be unity. The amplitude of the perturbation on η at the origin is normalized as

$$\eta_1 = 1 \quad \text{at} \quad x = 0 \tag{55}$$

Then, the problem is reduced to the one to solve (49)–(52) under the five boundary conditions, (53a–d) in addition to (54) and (55). This is solved with the use of the relaxation method[8].

5. Results and discussion

5.1 The dominant wavenumber and the profile of perturbation

Figure 4 shows the growth rate of perturbations Ω as functions of the wavenumber k. As found in the figure, Ω has common features to the previous study of self-preserving analysis[3]. The growth rate Ω asymptotically approaches zero in the limit $k \to 0$. In the range of moderate values of k Ω increases in the positive range with k and is maximized when $k = 0.1 \sim 1$. If k exceeds some value around unity, Ω becomes negative.

The dominant wavenumber k and the growth rate of perturbation Ω are found to increase with increasing curvature of the slope β. This implies that an increase in the acceleration of flow promotes channelization with smaller wavelength. This result agree with the result of the upstream-driven theory on a non-flat bed by Revelli and Ridolfi[4]. From their results, they concluded that the curvature gives a significant effect on the characteristic wavelength, and an increase in the downward-concave curvature corresponds to a decrease in the dominant wavelength.

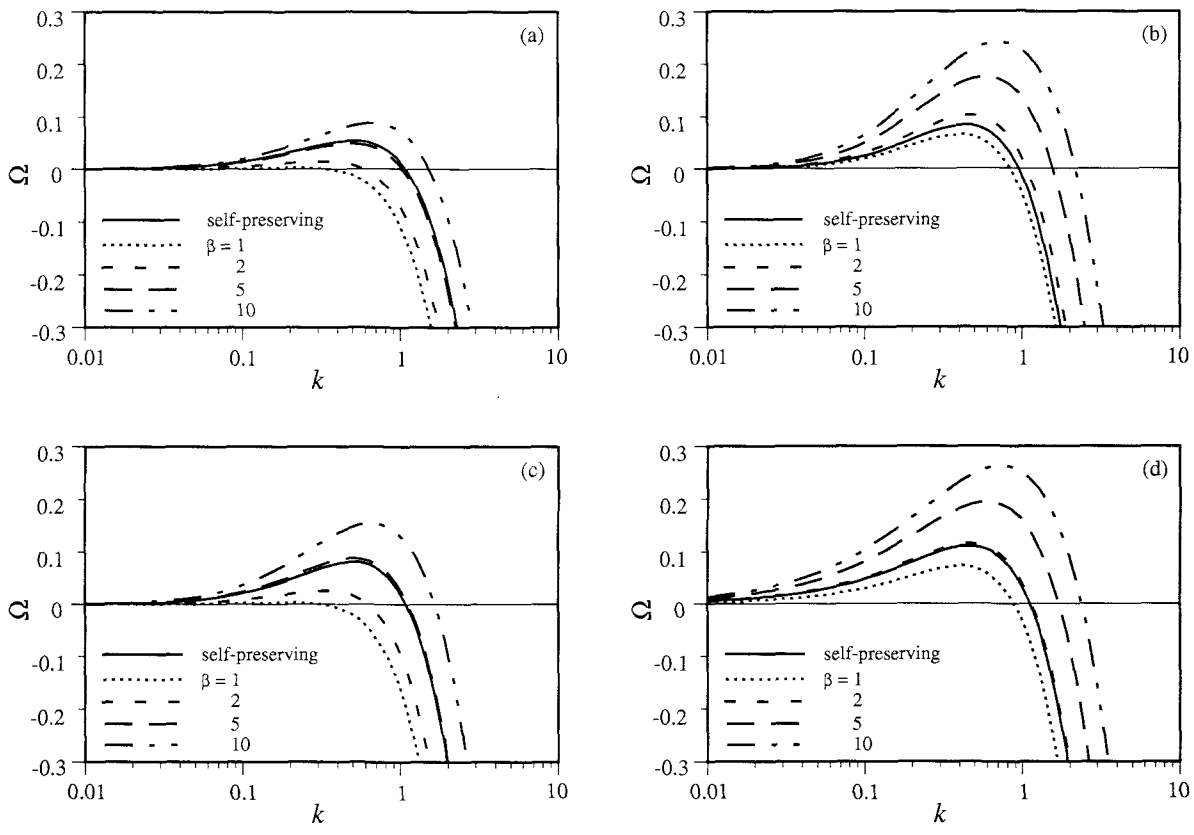

Fig. 4 The growth rate of perturbations Ω as function of k and β. (a) $\sigma = 0.1$, $\psi = 0.5$ and $\gamma = 1.5$. (b) $\sigma = 0.1$, $\psi = 0.3$ and $\gamma = 1.5$. (c) $\sigma = 0.1$, $\psi = 0.3$ and $\gamma = 2$. (d) $\sigma = 0$, $\psi = 0.3$ and $\gamma = 1.5$.

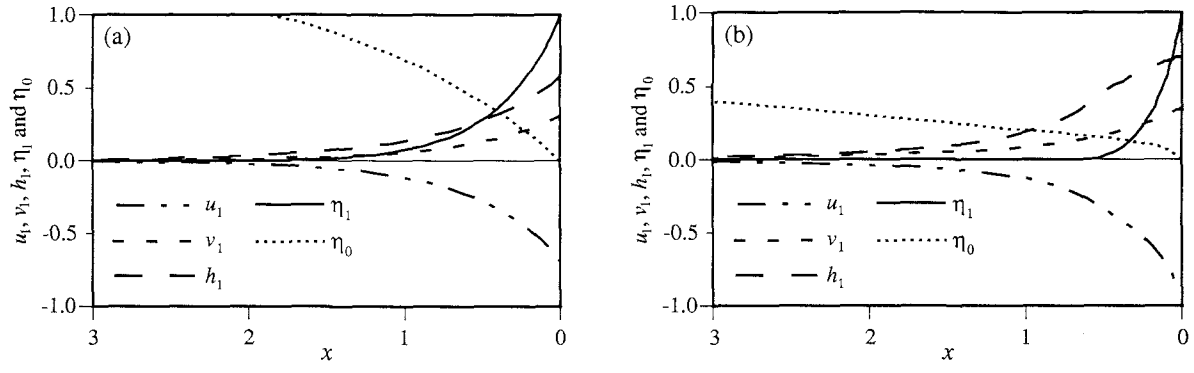

Fig. 5 Profiles of perturbations in the streamwise direction for $\sigma = 0.1$, $\psi = 0.5$, $\gamma = 1.5$, $k = 0.55$. (a) $\beta = 1$ and $\Omega = -0.017$. (b) $\beta = 10$ and $\Omega = 0.085$.

Comparing Fig. 4a and Fig. 4b, we found that a decrease in the normalized critical shear stress ψ strongly amplifies the growth rate Ω. Meanwhile, in the case of the self-preserving analysis, the critical shear stress ψ does not have a significant effect. This is probably because the self-preserving base state profile depends on ψ, so that the effect of ψ is absorbed by the profile. From Figs. 4b and 4c. the growth rate Ω is found to decrease with increasing exponent of the erosion function γ. This is also caused by the fact that the effect of γ is absorbed by the self-preserving base state profile. Comparing Fig. 4b with Fig. 4d, we find that Ω increases with decreasing σ in both analyses for arbitrary slope profiles and the self-preserving profile.

The examples of the profiles of the perturbations u_1, v_1, h_1, η_1, and the base state η_0 in the streamwise direction are shown in Fig.5. It is found that the

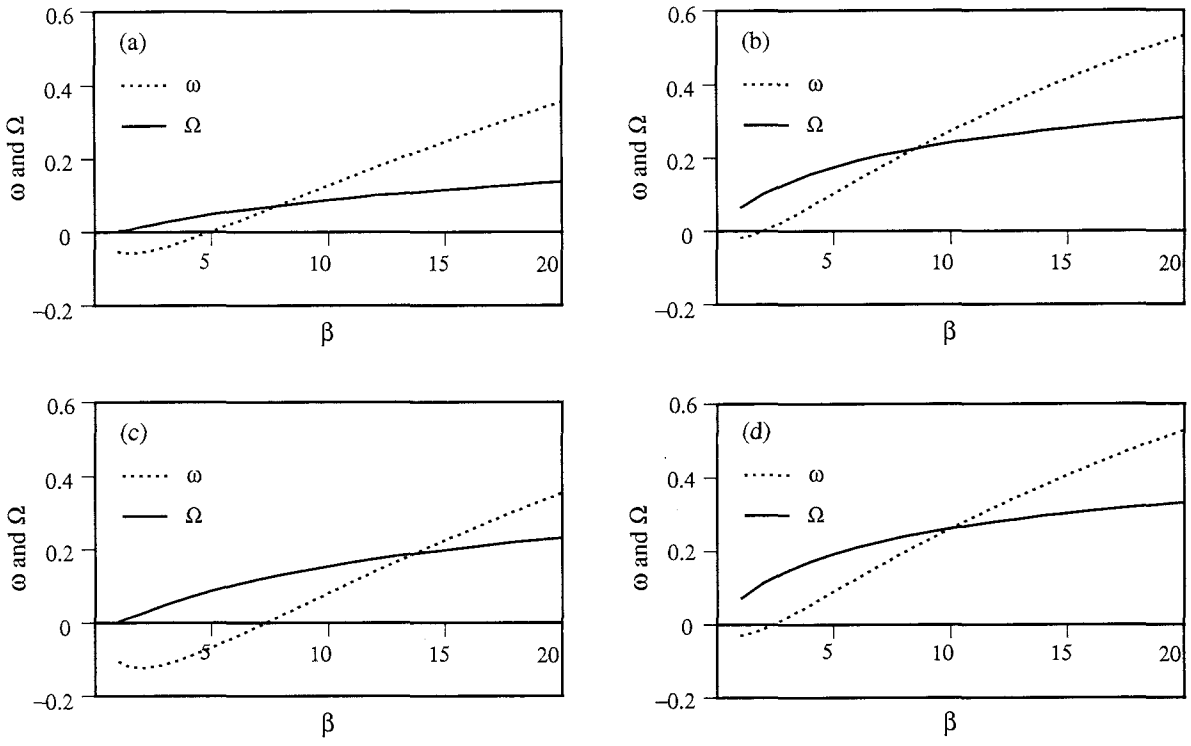

Fig. 6 Comparison between ω and Ω. (a) $\sigma = 0.1$, $\psi = 0.5$ and $\gamma = 1.5$. (b) $\sigma = 0.1$, $\psi = 0.3$ and $\gamma = 1.5$. (c) $\sigma = 0.1$, $\psi = 0.3$ and $\gamma = 2$. (d) $\sigma = 0$, $\psi = 0.3$ and $\gamma = 1.5$.

perturbations u_1, v_1 and h_1 in Fig. 5b ($\Omega = 0.085$) can penetrate further upstream than the ones in Fig. 5a ($\Omega = -0.017$).

5.2 The momentary stability concept

As mentioned in the Introduction, the criterion for stability needs to be studied in reference to the growth or decay of the evolving base state. In the momentary stability concept, the stability of the base state to perturbations at a given instant is evaluated by comparing the growth rate of perturbations with the evolution speed of the base state, both averaged over the whole domain. It should be noted that the results of this analysis are nevertheless invalid if the evolution speed of the base state is large ($|\partial\eta/\partial t| > 1$) because the time variation of the base state is neglected in the two-dimensional perturbation problem (the frozen time approach). It may be possible to obtain a higher order approximation by introducing asymptotic expansions with a parameter representing the time scale of evolution of the base state which must be sufficiently smaller than unity[9]. If the evolution of the base state is rapid, however, numerical simulation is the only method to study the stability of slopes.

In the analysis by Shen[5], the flow energy as an appropriate measure is employed to evaluate the instability of unsteady base flow. Meanwhile, the present analysis concerns the instability of bed profiles. We need to introduce an appropriate measure to quantify the stability of time-dependent base profiles. Since the normalized erosion represents the normalized bed evolution in the stationary coordinate as shown in Eq. (16), the intensities of erosion (erosion rate squared, E^2) may be a possible choice. We introduce the ratio between the erosion intensities of the base state as well as the perturbation in the form

$$\mathcal{E} = \frac{\int_{-\infty}^{0} E_1^2 \, \mathrm{d}x}{\int_{-\infty}^{0} (E_0 - E_n)^2 \, \mathrm{d}x} \tag{56}$$

where E_0 and E_1 denote the erosion rates of the base state and the perturbation respectively, and $\mathcal{E}$ is the ratio between the two.

Thus, the criterion for "momentary stability" of the time-dependent arbitrary base state, according to Shen[5], is written in the form

$$\mathcal{G} = \frac{1}{2\mathcal{E}} \frac{\mathrm{d}\mathcal{E}}{\mathrm{d}t} = \Omega - \omega \tag{57}$$

where Ω is the growth rate of perturbation, and ω is the growth rate of base state given by

$$\omega = \frac{\int_{-\infty}^{0} \left(E(u_0^2) - E_n\right) \frac{\partial E(u_0^2)}{\partial t} \mathrm{d}x}{\int_{-\infty}^{0} \left(E(u_0^2) - E_n\right)^2 \mathrm{d}x} \tag{58}$$

If $\mathcal{G} > 0$, the bed may be momentarily unstable, whereas if $\mathcal{G} < 0$, it may be momentarily stable. For the self-preserving profile, ω definitely vanishes.

Figure 6 shows comparisons between ω and Ω as functions of β from $\beta = 1$ to 20. It is found that when β increases, both ω and Ω increase. However, ω increases faster than Ω, so that, at some value of β, ω becomes larger than Ω. This means that the system becomes momentarily stable in the range of large β. From the momentary stability analysis, we can conclude that even if the slope does not have the self-preserving profile, channelization is possible when the curvature of the slope is not so large.

Let us consider flow on a broad and unchannelized plateau, which was unleveled by tectonic uplift or volcanic movement. In the beginning, the downstream end of the plateau can be rather angular, so that the curvature there is large. This corresponds to somewhere in the range of large β in Fig. 6a–d, where the base state is momentarily stable. Therefore, even though erosion is active at the downstream end of the plateau, no channelization takes place. As time progresses, flow induces erosion on the plateau especially in the vicinity of the downstream end. Thus, the angular edge gradually becomes smooth, and the curvature around the edge decreases. When the curvature (or β) becomes sufficiently small and Ω overcomes ω as shown in Fig. 6a–d ($\mathcal{G} = 0$), channelization begins. The dominant wavenumbers k_m corresponding to β where Ω becomes larger than ω in Fig. 6a–d are found to be 0.6, 0.7, 0.74 and 0.73, respectively, which are expected to be the wavenumbers of incipient channels.

The dimensional characteristic spacing between incipient channels $\tilde{\lambda}_m$ is described by

$$\tilde{\lambda}_m = \frac{2\pi \tilde{D}_c}{C_f k_m} \tag{59}$$

where k_m denotes the characteristic wavenumber.

From the results of momentary stability, k_m is approximately equal to 0.7. Let assume the friction coefficient C_f equal to 0.01. Thus, we got that the characteristic spacing $\tilde{\lambda}_m$ between incipient channels is on the order of one thousand times the Froude critical depth $\tilde{D}_c$. This result from the momentary stability analysis corresponds well to the result from the previous study[3]. Nevertheless, the present analysis points out the processes of channel inception that cannot be explained by the previous analysis.

6. Conclusion

The linear stability analysis of channelization on slopes with time-dependent arbitrary shapes in the purely erosional case is performed. It is found that, even if the base state bed profile is not the self-preserving profile assumed in the existing analysis[3], the channelization can occur on slopes. The growth rate of perturbation increases and the dominant wavelength decreases with increasing curvature of slopes. Applying the concept of "momentary stability", we found slopes become momentarily stable in the range of large curvatures.

Acknowledgement

This study was supported by the Foundation of Hokkaido River Disaster Prevention Research Center.

REFERENCES

1) Smith, T. and F. B. Bretherton: Stability and the conservation of mass in drainage basin evolution, *Wat. Resour. Res.*, Vol. 8, pp. 1506–1529, 1972.
2) Izumi, N. and G. Parker: Inception of channelization and drainage basin formation: upstream-driven theory, *J. Fluid Mech.*, Vol. 283, pp. 341–363, 1995.
3) Izumi, N. and G. Parker: Linear stability analysis of channel inception: downstream-driven theory, *J. Fluid Mech.*, Vol. 419, pp. 239–262, 2000.
4) Revelli, R. and L. Ridolfi: Inception of channelization over a non-flat bed, *Meccanica*, Vol. 35, pp. 457–461, 2000.
5) Shen, S. F.: Some considerations on the laminar stability of time-dependent basic flows, *J. Aero. Sci.*, Vol. 28, pp. 397–404, 417, 1961.
6) Chen, C. F. and R. P. Kirchner: Stability of time-dependent rotational Couette flow. part 2. stability analysis, *J. Fluid Mech.*, Vol.48, pp. 365–384, 1971.
7) Matar, O. K. and S. M. Troian: The development of transient fingering patterns during the spreading of surfactant coated films, *Phys. Fluids*, Vol. 11(11), pp. 3232–3246, 1999.
8) Press, H. P., S. A. Teukolsky: W. T. Vetterling and B. P. Flannery: *Numerical Recipes in FORTRAN*, 2nd ed, Cambridge, 1992.
9) Rosenblat, S. and D. M. Herbert: Low-frequency modulation of thermal instability, *J. Fluid Mech.*, Vol. 43, Part 2, pp. 385–398, 1970.

(Received April 16, 2004)